

## EVAPORATION DUCT RETRIEVAL USING CHANGES IN RADAR SEA CLUTTER POWER VERSUS RECEIVING HEIGHT

J.-P. Zhang<sup>1</sup>, Z.-S. Wu<sup>1,\*</sup>, Y.-S. Zhang<sup>2</sup>, and B. Wang<sup>3</sup>

<sup>1</sup>School of Science, Xidian University, Xi'an 710071, China

<sup>2</sup>China Research Institute of Radio Wave Propagation, Qingdao 266107, China

<sup>3</sup>Institute of Oceanographic Instrumentation, Shandong Academy of Sciences, Qingdao 266001, China

**Abstract**—A method for retrieving evaporation duct height (EDH) is introduced in this paper. The proposed technique employs the changes in radar sea clutter power observed at different heights as input information. It identifies the EDH associated with the modeled clutter change pattern that best matches measured change patterns. The performance of the method is evaluated in terms of RMS errors in retrieving actual EDHs that range from 0 to 40 m. The comparison of the proposed method with the conventional clutter pattern matching method shows that the former more effectively retrieves actual EDHs.

### 1. INTRODUCTION

An evaporation duct is a quasi-permanent anomalous structure of the atmospheric refractivity frequently encountered in open oceans and coastal zones. It is created by rapid anomalous changes in the vertical atmospheric temperature and humidity gradients immediately above water masses [1, 2]. Many nonstandard propagation events can be induced by this ducting condition, including over-the-horizon detection, radar holes where the radar is effectively blind and positioning failure [3–5]. Accordingly, understanding the atmospheric environment is essential in evaluating and predicting the performance of maritime radar and communication systems.

The modified refractivity profile of an evaporation duct is classically modeled using the log-linear Paulus-Jeske model [2, 6], in

---

*Received 13 December 2011, Accepted 19 March 2012, Scheduled 5 April 2012*

\* Corresponding author: Zhen-Sen Wu (wuzhs@mail.xidian.edu.cn).

which evaporation duct height (EDH) is the only parameter that determines duct strength. Various traditional methods have been used to determine the atmospheric refractivity profile; these approaches include “bulk” models with in situ measurements as input, microwave refractometers [7], LIDAR techniques [8], and many numerical weather prediction models [9]. In recent years, a technique referred to as refractivity from clutter (RFC) has been widely used in retrieving the refractivity profile in maritime environments [10–14]. This method can easily be performed without additional instruments apart from the radars installed on ships. The refractivity profile with high temporal and spatial resolution can then be inferred from radar clutter returns. The RFC technique has been successfully applied to the inversion of evaporation duct profiles (i.e., EDHs). To estimate EDH from radar sea clutter observations, Rogers et al. [10] used a nonlinear least squares inversion procedure, which was tested with data from an experiment conducted at Wallops Island, Virginia, in 1998. Yardim et al. [15] tracked the temporal and spatial evolution of evaporation duct parameters from radar sea clutter using an extended Kalman filter. Later, they investigated the performance of an evaporation duct RFC estimator by introducing an error metric as a function of the radar parameters, sea surface characteristics, and the environment; the authors also developed a Bayesian estimator that incorporates meteorological statistics into RFC inversion [16,17]. Very recently, Karimian et al. [18] provided a good review of the many applications of the RFC technique.

The RFC technique identifies the best atmospheric refractivity profile by matching measured radar clutter power patterns with those predicted by forward propagation models. In retrieving the modified refractivity profile for an evaporation duct, this technique is generally performed on the basis of the clutter power received at a fixed antenna height, as in Rogers et al. [10], Yardim et al. [17], and Wang et al. [19]. That is, only one observed clutter power pattern is used as input into an RFC inversion algorithm. In the present study, this implementation approach of the RFC is referred to as the “clutter pattern matching” (CPM) method. Because limited clutter information is employed, inferring the evaporation duct profile by the CPM method is difficult in some cases. For example, some actual EDHs are difficult to retrieve when sea clutter is measured by a radar system with inappropriate frequency and antenna height. Therefore, more sources of radar clutter observations are necessary to improve RFC performance in EDH retrieval.

In this paper, we introduce a new EDH retrieval method, which takes advantage of radar sea clutter received at various heights. The

inspiration behind this method primarily stems from the significant influence of antenna height on the clutter library of an evaporation duct; this influence results in different RFC performance levels. The simplest approach to performing inversion using multiple observed clutter patterns is multi-objective optimization, but we do not adopt this method because of its mechanicalness. We found that changes in the power of radar sea clutter returns, as a function of receiving height, exhibit good sensitivity to EDHs. Consequently, the clutter change pattern resulting from these power changes can be used to retrieve EDHs. This method, referred to as the “clutter change pattern matching” (CCPM) method in this paper, is developed in Section 4. The corresponding EDH inversion model is also presented. The performance analysis discussed in Section 5 shows that the CCPM method more effectively retrieves most actual EDHs than does the conventional CPM method.

## 2. FORWARD MODELING

### 2.1. Radio Refractivity Environment Model

A radio refractive environment is commonly described by atmospheric refraction index  $n$ , which is dependent on atmospheric pressure, temperature, and water vapor pressure. The value of  $n$  is typically 1.00035 at the Earth’s surface, but varies, with its height rarely exceeding  $\sim 1.0004$  [20]. This minimal variation enables a more convenient description of the refractive index in terms of refractivity  $N$ , defined by

$$N = (n - 1) \times 10^6. \quad (1)$$

The radio refractive environment can be classified into standard, subrefraction, superrefraction, and ducting environments. Ducting environments are those associated with refractive conditions for which  $dN/dh < -0.157N$ -units/m. To take the effects of the Earth’s curvature into account, we introduce a modified refractivity  $M$ , defined as  $M = N + 0.157z$  [20], where  $z$  is the height above the mean sea level.  $M$  can identify ducting (trapping) gradient regions more clearly because ducting occurs when  $dM/dz < 0$ . In ducting environments, radio rays are bent toward the surface of the Earth more rapidly than at the Earth’s curvature. These rays are also trapped for an extended range. Three typical types of atmospheric ducts exist: evaporation, surface-based, and elevated ducts [20, 21]. Evaporation ducts are created by the rapid decrease in moisture immediately adjacent to the ocean surface, and are nearly permanent propagation mechanisms for the radar waves propagating over the ocean surface. The occurrence

probability of an evaporation duct is up to 89 % at the South China Sea [22].

Electromagnetic wave propagation modeling and atmospheric refractivity environment estimation necessitate a parametric refractivity profile model [23]. The modified refractivity profile for an evaporation duct is usually simulated using the log-linear Paulus-Jeske model [2, 6] as follows:

$$M(z) = M_0 + 0.125z - 0.125\delta \ln\left(\frac{z + z_0}{z_0}\right), \quad (2)$$

where  $z$  is the height (m) above the mean sea level;  $\delta$  denotes the EDH (m) which is the top height of the trapping layer;  $z_0$  is an aerodynamic roughness factor whose typical overwater value is  $1.5 \times 10^{-4}$  m;  $M_0$  represents the modified refractivity at the sea surface. Because the radio wave propagation depends on the vertical and horizontal gradients of the modified refractivity not on its absolute value,  $M_0$  is taken as a typical value 339 M-units in this study. The Paulus-Jeske model is derived under neutral stability conditions (i.e., the difference between air and sea surface temperatures is nearly zero) and used for all EDH inversions in this paper.

## 2.2. Radar Wave Propagation Modeling

The RFC of an evaporation duct is an inverse estimation problem; thus, the RFC technique has to be implemented on the basis of a forward calculation model, i.e., a radar wave propagation model. The performance of this model heavily affects estimation results.

Given an atmospheric refractivity structure  $\mathbf{M}$  in a maritime environment, the received radar sea clutter power can be modeled by a monostatic radar equation:

$$P_c(x, \mathbf{M}) = \frac{P_t G_t^2 \lambda^2 \sigma_0(x) A_c(x)}{(4\pi)^3 x^4} \cdot F^4(x, \mathbf{M}), \quad (3)$$

where  $x$  is the range from the radar transmitter,  $P_t$  denotes the transmitter power,  $G$  is the antenna gain,  $\lambda$  represents the wavelength,  $A_c$  is the radar cell area, and  $F$  is the pattern propagation factor.  $\sigma_0$  denotes the backscattering coefficient of the ocean surface [24–29], calculated using the GIT model [2] in this work.

The pattern propagation factor accounts for the effect of refractivity structure  $\mathbf{M}$  and the pattern function of the transmitting antenna. We model this factor using a parabolic equation (PE) method [30]. The final form of the PE [31, 32] is

$$\partial_z^2 u + 2ik\partial_x u + k^2 \left( n^2 - 1 + \frac{2z}{a_e} \right) u = 0, \quad (4)$$

where  $u(x, z)$  is the electromagnetic field component at range  $x$  and height  $z$ ,  $k$  is the wave number, and  $n$  denotes the index of refraction of the atmosphere.  $2z/a_e$  accounts for the spherical shape of the Earth; when it is disregarded, (4) describes the propagation over a flat Earth. The PE has a mixed Fourier split-step solution [31]:

$$u(x, z) = e^{ikm\Delta x/2} \left\{ e^{i\alpha^2\Delta x/2k} e^{-\alpha z} K(x_0) + \frac{2}{\pi} \int_0^\infty \frac{\alpha \sin pz - p \cos pz}{\alpha^2 + p^2} e^{-ip^2\Delta x/2k} \cdot \int_0^\infty u(x_0, z') [\alpha \sin pz' - p \cos pz'] dz' dp \right\}, \quad (5)$$

where  $\Delta x$  is the range step in PE,  $p = k \sin \theta$  is the transform variable ( $\theta$  is the angle from the horizontal), and  $m(x, z)$  is the modified refractivity term at the 2D space  $(x, z)$ . The definitions of the other parameters can be found in Kuttler and Dockery [31, 33].

In terms of split-step field  $u$ , we can express the pattern propagation factor in a rectangular coordinate system as follows:

$$F = \sqrt{x} |u(x, z)|, \quad (6)$$

where  $x$  is the distance between the point of interest and radar transmitter.

The radar clutter power given by (3) can be simply expressed using one-way path loss  $L(x, \mathbf{M})$  thus:

$$P_c(x, \mathbf{M}) = -2L(x, \mathbf{M}) + \sigma^0(x) + 10 \log_{10}(x) + C, \quad (7)$$

with

$$L(x, \mathbf{M}) = 32.44 + 20 \log_{10} f(\text{MHz}) + 20 \log_{10} x(\text{km}) - 20 \log_{10} F(x, \mathbf{M}), \quad (8)$$

where  $f$  is the radar frequency in MHz, and  $C$  is a constant that depends on the radar parameters, expressed as

$$C = P_t(\text{dB}) + 2G_t(\text{dB}) + 10 \log_{10} (4\pi \cdot \theta_{AZ} \cdot \sec \varphi \cdot \Delta r / 2\lambda^2), \quad (9)$$

with  $\theta_{AZ}$  as the azimuth beam width (radian),  $\varphi$  as the grazing angle (radian),  $\Delta r$  as the radar range bin width (m), and  $\lambda$  as the wavelength (m).  $P_c$  and  $L$  in (7) and (8) are in dB.

Two examples of radar wave propagation in evaporation duct environments are shown in Fig. 1. The frequency is 10 GHz. The diagrams show that the path loss is significantly reduced by the evaporation duct, and that the trapping phenomenon occurs in these conditions.

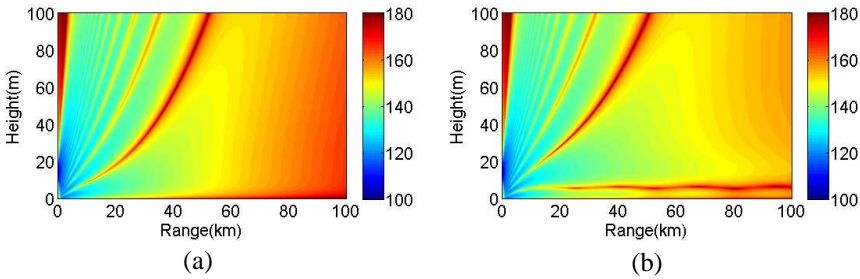


**Figure 1.** One-way path loss  $L$  (dB) diagram for two evaporation duct environments. (a) EDH = 10 m and (b) EDH = 20 m. The transmitter antenna is taken at 15 m above the mean sea level, vertically polarized and horizontally oriented toward the ocean surface with a beam width of  $0.7^\circ$ .

**Table 1.** Radar system parameters.

Parameter	Value
Power, dBm	80.0
Antenna gain, dB	40.0
Beam width, deg	0.7
Range bin width, m	200.0
Elevation, deg	0.0
Polarization	VV
Beam pattern	Gaussian

### 3. CLUTTER PATTERN MATCHING METHOD

The conventional CPM method for evaporation duct RFC inversion identifies the EDH associated with the clutter pattern (in the modeled clutter library) that best matches the observed clutter pattern. The match between the modeled and observed clutter patterns is normally quantified by an objective function used in optimization. The structure of the modeled clutter library determines the sensitivity of the objective function to the EDH, and therefore determines how well the CPM method performs in a given evaporation ducting environment.

The clutter libraries for three radar frequencies and four antenna heights are shown in Fig. 2. The other radar system parameters used in the clutter power predictions are listed in Table 1. Wind speed and direction are assumed to be 8 m/s and upwind, respectively. These conditions correspond to an average wave height  $h_{av} = 0.82$  m ( $h_{av} = (V_w/8.67)^{2.5}$ ) and wind direction  $\phi = 180^\circ$  which are used in

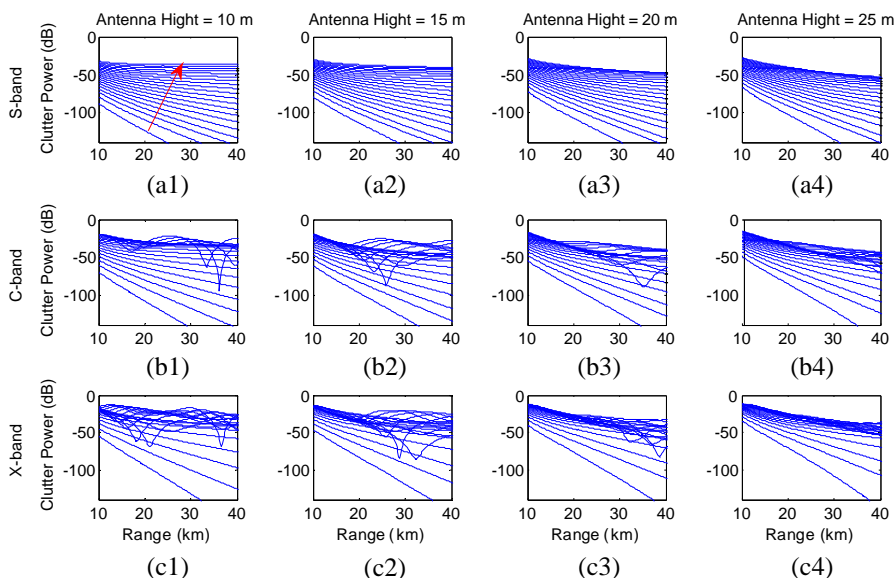


**Figure 2.** Clutter libraries of evaporation ducts with EDHs ranging from 2 to 40 m, in 2 m increments, for radar frequencies of 3, 6, and 10 GHz (for S-, C-, and X-bands, respectively), and antenna heights of 10, 15, 20, and 25 m above the mean sea level. The red arrow shows the evolution of the clutter pattern as EDH increases.

the scattering coefficient calculation by the GIT model. The different radar frequency–height combinations result in different structures of and variations in the clutter library. Figs. 2(a1)–2(a4) shows that the clutter power pattern for S-band monotonically increases with increasing EDH. However, the rate of power increase gradually decreases and the clutter patterns that correspond to larger EDHs converge to almost the same value. The larger the antenna height, the faster the convergence. The low sensitivity of the clutter pattern to larger EDHs causes difficulty in EDH retrieval. As the radar frequency increases, the structure of the clutter library becomes more complex, as shown in Figs. 2(b1)–2(b4) (C-band) and Figs. 2(c1)–2(c4) (X-band). In these cases, the clutter pattern first monotonically increases as EDH rises to a critical value, and is then dominated by constructive/destructive interference. This pattern change is beneficial to the retrieval of numerous EDHs, except those near the critical value. At an antenna height of 25 m, the libraries (Figs. 2(b4) and 2(c4)) have structures similar to that of the S-band radar.

The effect of the different clutter library structures (resulting from different radar frequency–height combinations) on the evaporation

duct RFC performance is usually quantified by the objective function used in inversion. A conventional objective function used in previous EDH inversion research is the least squares error function (LSEF) [11], defined as

$$\phi(\mathbf{m}) = \sum_{x=x_0}^{x_f} e^2(x), \quad (10)$$

with

$$e(x) = P_c^{obs}(x) - P_c(x, \mathbf{m}) - \left[ \bar{P}_c^{obs} - \bar{P}_c(\mathbf{m}) \right], \quad (11)$$

$$\bar{P}_c^{obs} = \frac{1}{N_x + 1} \sum_{x=x_0}^{x_f} P_c^{obs}(x), \quad (12)$$

$$\bar{P}_c(\mathbf{m}) = \frac{1}{N_x + 1} \sum_{x=x_0}^{x_f} P_c(x, \mathbf{m}), \quad (13)$$

where  $\mathbf{m}$  represents the environmental parameter vector to be retrieved, which in effect contains only one parameter (EDH) for the evaporation ducting environment (2).  $x_0$  and  $x_f$  are the initial and final ranges of the clutter returns used in inversion, and  $N_x$  is the number of the range bins in this range interval.  $\bar{P}_c^{obs}$  and  $\bar{P}_c(\mathbf{m})$  are the means of the observed and modeled clutter power, respectively; they are introduced here so that the objective function depends only on the variation in clutter power but not on the absolute power level.

Different objective function sensitivities to EDHs result in varied retrieval qualities. The LSEF sensitivity characteristics that correspond to the clutter libraries given in Fig. 2 are shown in Fig. 3. Three actual EDHs (i.e., objective EDHs for retrieval) — 10, 20, and 30 m — are considered for each radar frequency–height combination. One can see that the objective functions that correspond to the three actual EDHs have different EDH sensitivities. These differences result in varied levels of inversion for a certain frequency–height combination in retrieving the different EDHs. That is, the actual EDHs are retrieved under varying levels of difficulty given a certain radar frequency and antenna height. For example, retrieving the EDHs from 20 to 30 m at a radar frequency of 6 GHz and an antenna height of 10 m involves hard work (Fig. 3(b1)). Comparing all the subfigures in Fig. 3 shows that for different radar systems (frequency–height combinations), the objective function that corresponds to an actual EDH exhibits different EDH sensitivities, thereby generating varied levels of performance for these radar systems in retrieving the EDH. If the actual EDH is 30 m, for example, a frequency–height combination of 6 GHz–15 m (Fig. 3(b2))

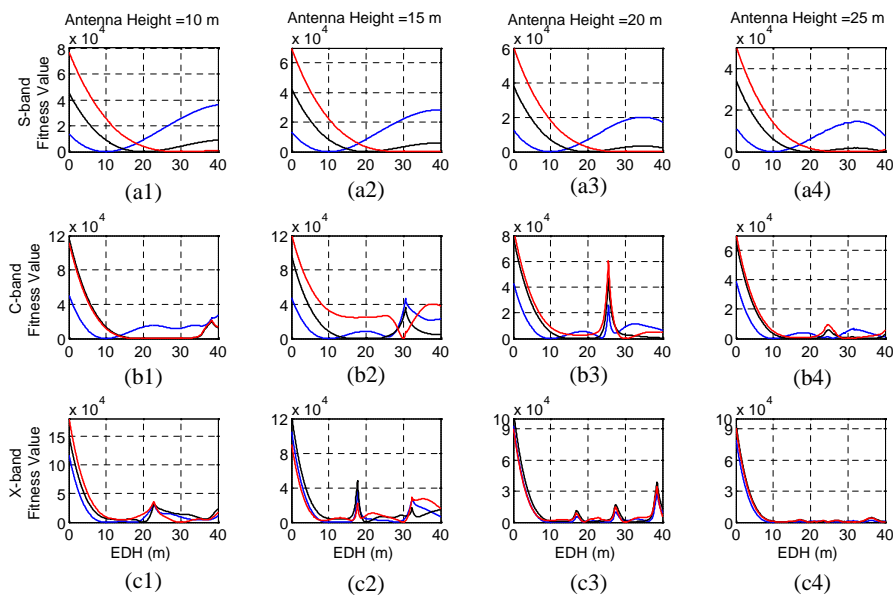


**Figure 3.** Least squares error function that correspond to the clutter libraries given in Fig. 2 for three actual EDHs (i.e., objective EDHs for retrieval): (blue line) 10 m, (black line) 20 m, and (red line) 30 m.

may yield better performance than do other combinations because of the distinct minimum at a 30 m EDH.

#### 4. CLUTTER CHANG PATTERN MATCHING METHOD

##### 4.1. Clutter Chang Pattern and Objective Function

The different performance levels generated by a given frequency–height combination in retrieving different actual EDHs and by different frequency–height combinations in retrieving a given EDH (illustrated in Section 3) indicate that retrieving all possible actual EDHs (0–40 m) using the sea clutter from only one frequency–height combination (i.e., the CPM method) is difficult to achieve in certain cases. EDH inversion quality can be improved by combining the sea clutter from multiple radar frequency–height combinations. In this section, we introduce an EDH inversion method, which works on the basis of the changes in the power pattern of radar sea clutter as receiving height increases. This technique is referred to as the CCPM method.

Let us assume that the receiving height increases from 9 to 25 m in 0.5 m increments. The sea clutter change pattern libraries for three radar frequency bands (*S*, *C*, and *X*) are shown in Fig. 4. The mean

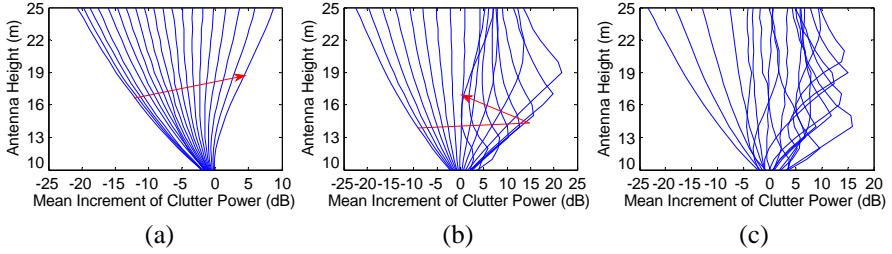


**Figure 4.** Mean increments between clutter powers received at a 10 to 25 m height and those received at 9 m within evaporation ducts with EDHs ranging from 2 to 40 m in 2 m increments. (a) 3 GHz, (b) 6 GHz, and (c) 10 GHz. The red arrows show the evolution of the clutter change pattern as EDH increases.

increment of clutter power refers to the average variation in clutter power in the inversion range interval (taken as 10–40 km in this work). The other radar parameters used are the same as those shown in Fig. 2. The clutter change pattern library for S-band (Fig. 4(a)) consists of change patterns with monotonically varying vertical slopes as EDH increases. This monotonic and distinct variation in the vertical slope results in good sensitivity to different EDHs. The C- and X-band libraries (Figs. 4(b) and 4(c)) have more complex structures because the vertical slope of the clutter change pattern becomes more intricate as EDH increases. Despite this slope complexity, the differences between these patterns are clearly observable. Thus, good EDH sensitivity may also exist.

The EDH sensitivities described above suggest that the actual EDH can be retrieved by matching the measured clutter change pattern and that derived by a forward model. The EDH associated with the best match is our expected inversion result. We introduce the newly defined LSEF as the objective function to quantify the match in this scenario:

$$\Phi(\mathbf{m}) = \sum_{h=h_0}^{h_f} \left\{ \Delta P_c^{obs}(h) - \Delta P_c(h, \mathbf{m}) - \left[ \overline{\Delta P_c^{obs}} - \overline{\Delta P_c(\mathbf{m})} \right] \right\}^2, \quad (14)$$

with

$$\Delta P_c^{obs}(h) = \frac{1}{N_x + 1} \sum_{x=x_0}^{x_f} \left[ P_c^{obs}(h_0, x) - P_c^{obs}(h, x) \right], \quad (15)$$

$$\Delta P_c(h, \mathbf{m}) = \frac{1}{N_x + 1} \sum_{x=x_0}^{x_f} \left[ P_c(h_0, x, \mathbf{m}) - P_c(h, x, \mathbf{m}) \right], \quad (16)$$

$$\overline{\Delta P_c^{obs}} = \frac{1}{N_h - 1} \sum_{h=h_0}^{h_f} [\Delta P_c^{obs}(h)], \tag{17}$$

$$\overline{\Delta P_c(\mathbf{m})} = \frac{1}{N_h - 1} \sum_{h=h_0}^{h_f} [\Delta P_c(h, \mathbf{m})], \tag{18}$$

where  $h_0$  and  $h_f$  are the initial and final receiving heights of the sea clutter returns, and  $N_h$  is the number of antenna heights in this height interval.  $\overline{\Delta P_c^{obs}}$  and  $\overline{\Delta P_c(\mathbf{m})}$  denote the means of the observed (measured) and modeled mean increments of clutter power  $\Delta P_c^{obs}(h)$  and  $\Delta P_c(h, \mathbf{m})$ , respectively. The rest of the parameters have the same definitions as those in (10)–(13).

The EDH sensitivity characteristics (which correspond to the three clutter change pattern libraries shown in Fig. 4) of the new objective function given by (14) are shown in Fig. 5. The red circles indicate the locations of the minimum fitness value. This objection function achieves global minima for the three cases only at the actual EDHs, indicating good EDH sensitivity, which in turn, results in robust inversion. However, at 10 GHz (Fig. 5(c)), the objection function has a local minimum at an EDH of approximately 24 m (denoted by a red square), which is very close to the global minimum at an observed EDH of 10 m. This result may diminish inversion quality when the actual EDH is about 10 m.

The performance of the CCPM method, in which the new objective function is used, is illustrated in Section 5.

### 4.2. Inversion Model

The CCPM method can be employed to develop the evaporation duct inversion model, i.e., the EDH retrieval procedure, described as follows:

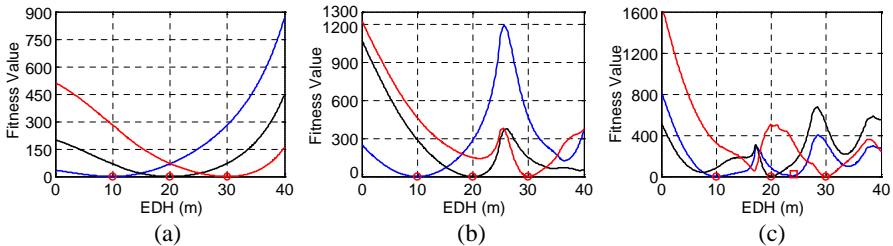


**Figure 5.** New least squares error function (14) that corresponds to the clutter change pattern libraries given in Fig. 4, for three actual EDHs (i.e., objective EDHs for retrieval): (blue line) 10 m, (black line) 20 m, and (red line) 30 m. The radar frequencies are (a) 3 GHz, (b) 6 GHz, and (c) 10 GHz.

1) The observed sea clutter returns received at height interval  $[h_0, h_f]$ , i.e.,  $P_c^{obs}(h, x)$  in (15) are obtained.

2) Mean increments  $\Delta P_c^{obs}(h)$  between the observed clutter powers received at different heights  $P_c^{obs}(h, x)$  and those received at initial height  $P_c^{obs}(h_0, x)$  are calculated.

3) Evaporation ducting environment  $\mathbf{M}$  is modeled; that is, a parameter vector  $\mathbf{m}$  of the evaporation duct M-profile is identified for retrieval. In this paper, the evaporation duct is simulated by the Paulus-Jeske model given by (2). Thus, the dimension of  $\mathbf{m}$  is 1, containing only the EDH.

4) The sea clutter returns received at height interval  $[h_0, h_f]$ , i.e.,  $P_c(h, x, \mathbf{m})$  in (16), are predicted using the forward propagation model provided in Section 2.

5) Mean increments  $\Delta P_c(h, \mathbf{m})$  between the predicted clutter powers received at different heights  $P_c(h, x, \mathbf{m})$  and those received at initial height  $P_c(h_0, x, \mathbf{m})$  are calculated. The mean increments for different EDHs make up the clutter change pattern library.

6) The objective function is constructed using (14) to quantify the fit of  $\Delta P_c(h, \mathbf{m})$  in  $\Delta P_c^{obs}(h)$ .

7) The objective function is optimized using an optimization algorithm. The EDH associated with the minimum fitness value is regarded as the inversion result.

## 5. PERFORMANCE ANALYSIS

In this section, we evaluate the performance of the CCPM method in retrieving EDHs. To this end, we compare the proposed method with the CPM approach. The inversion results presented here are in accordance with the inversion scenarios discussed in Sections 3 and 4. These results are based on a particle swarm optimization [34, 35] inversion algorithm.

The performance of the two EDH retrieval methods is illustrated using the RMS errors in the inversion of evaporation ducts, with actual EDHs ranging from 0 to 40 m (Fig. 6). The RMS errors are based on 1000 inversion realizations and defined as

$$\text{RMS}_{\delta_{actual}} = \left[ \frac{1}{n} \sum_{i=1}^n (\delta_i - \delta_{actual})^2 \right]^{1/2}, \quad (19)$$

where  $\delta_{actual}$  and  $\delta_i$  denote the actual and  $i$ -th retrieved EDHs, respectively. Because the clutter statistical characteristics affect the evaporation duct estimation significantly [17], we consider it in the actual clutter power modeling. The  $K$ -distribution was introduced as

an effective means to represent the sea clutter amplitude, and is used extensively in applications with low grazing angles. This distribution is used in this paper to account for the low grazing nature of the RFC. Besides, because of the low-resolution nature of the RFC, very spiky clutter is less likely to be encountered in RFC applications. The clutter is expected to be mildly to weakly spiky with the shape factor  $v = 1-5$  for most RFC applications [17]. For generality, the shape factor  $v$  is taken as 2.5 in this study.

The results of the CCPM method shown in Fig. 6 are generated on the basis of the radar sea clutters received at heights ranging from 10 to 25 m. For each radar frequency, these results are compared with four results of the CPM approach generated at four different antenna heights (10, 15, 20, and 25 m). The visual inspection shows that under a 3 GHz radar system, the CCPM method performs well for all the actual EDHs according to the small RMS errors (Fig. 6(a)). In this case of radar frequency, CCPM is more advantageous in retrieving high EDHs because the CPM method yields larger RMS errors in the

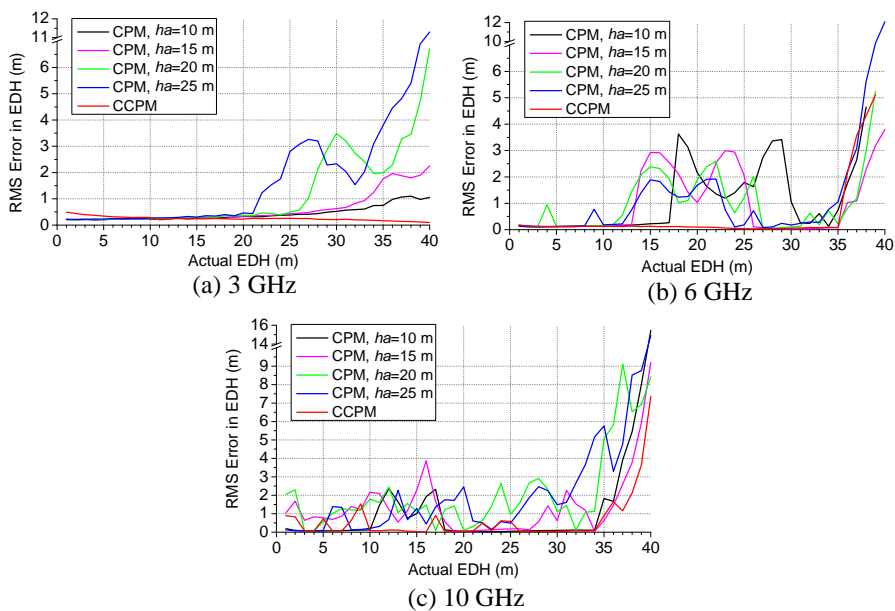


**Figure 6.** Performance plots for the clutter pattern matching method and the clutter change pattern matching method. The RMS EDH errors of the CPM method using radar antennas located at heights of (black lines) 10 m, (magenta) 15 m, (green) 20 m, and (blue) 25 m; the RMS EDH errors of (red lines) of the CCPM method. Three radar frequencies are tested: (a) 3 GHz, (b) 6 GHz, and (c) 10 GHz.

inversion of EDHs that are higher than approximately ( $ha = 10$  m) 33 m, ( $ha = 15$  m) 33 m, ( $ha = 20$  m) 27 m, and ( $ha = 25$  m) 21 m. This result is supported by the sensitivity of the objective function (Fig. 3(a)). The comparison of the two methods under a 6 GHz radar system is illustrated in Fig. 6(b). For actual EDHs lower than 35 m, CCPM performs better than does CPM. The large RMS errors of the CPM method for actual EDHs between 13 and 30 m result from the low EDH sensitivities of the objective function (Fig. 3(b)); these errors are effectively mitigated by the CCPM method. For actual EDHs higher than 35 m, however, both the proposed and CPM method produce biased results. The performance of the two EDH retrieval methods under a 10 GHz radar system (Fig. 6(c)) is similar to that under a 6 GHz radar system (Fig. 6(b)). In this case, one should note that the RMS EDH error of the CCPM method has a relatively high value at an actual EDH of about 9 m. This phenomenon is attributed to the local minimum of the objective function at the  $\sim 24$  m EDH (denoted by a red square in Fig. 5(c)).

Overall, the CCPM method more effectively retrieves most EDHs than does the CPM method. Although the proposed approach exhibits poor performance for actual EDHs higher than 35 m under a 6 or 10 GHz radar system, it is still the recommended method because an evaporation duct with very high EDH rarely occurs.

## 6. CONCLUSION

On the basis of good EDH sensitivity of the power change of radar sea clutter versus receiving height, we introduce a new EDH inversion method. It identifies actual EDHs by matching measured clutter change patterns and those predicted by forward propagation models. This method is called clutter change pattern matching (CCPM). The performance analysis indicates that the CCPM method has smaller RMS errors than does the conventional clutter pattern matching method in the inversion of most actual EDHs. This result suggests more effective EDH retrieval. The factor that restricts the application of this method is that the employed radar system requires a variable-height antenna.

## ACKNOWLEDGMENT

This research was supported by the National Natural Science Foundation of China under Grants 61172031 and 41175012.

## REFERENCES

1. Hitney, H. V., J. H. Richter, R. A. Pappert, et al., "Tropospheric radio propagation assessment," *Proc. IEEE*, Vol. 73, No. 2, 265–283, 1985.
2. Paulus, R. A., "Evaporation duct effects on sea clutter," *IEEE Trans. Antennas Propag.*, Vol. 38, No. 11, 1765–1771, 1990.
3. Yardim, C., P. Gerstoft, and W. S. Hodgkiss, "Estimation of radio refractivity from radar clutter using Bayesian Monte Carlo analysis," *IEEE Trans. Antennas Propag.*, Vol. 54, No. 4, 1318–1327, 2006.
4. Woods, G., A. Ruxton, C. Huddleston-Holmes, et al., "High-capacity, long-range, over ocean microwave link using the evaporation duct," *IEEE J. Ocean. Eng.*, Vol. 34, No. 3, 323–329, 2009.
5. Alexopoulos, A., "Effect of atmospheric propagation in RCS predictions," *Progress In Electromagnetics Research*, Vol. 101, 277–290, 2010.
6. Jeske, H., "State and limits of prediction methods of radar wave propagation conditions over sea," *Modern Topics in Microwave Propagation and Air-Sea Interaction*, 130–148, 1973.
7. Richter, J. H., "Sensing of radio refractivity and aerosol extinction," *International Geoscience and Remote Sensing Symposium*, Vol. 1, 381–385, Pasadena, CA, Aug. 8–12, 1994.
8. Willitsford, A. and C. R. Philbrick, "Lidar description of the evaporative duct in ocean environments," *Proc. SPIE*, Vol. 5885, 140–147, Bellingham, WA, 2005.
9. Haack, T. and S. D. Burk, "Summertime marine refractivity conditions along coastal California," *J. Appl. Meteorology*, Vol. 40, No. 4, 673–687, 2001.
10. Rogers, L. T., C. P. Hattan, and J. K. Stapleton, "Estimating evaporation duct heights from radar sea echo," *Radio Sci.*, Vol. 35, No. 4, 955–966, 2000.
11. Gerstoft, P., L. T. Rogers, J. L. Krolik, et al., "Inversion for refractivity parameters from radar sea clutter," *Radio Sci.*, Vol. 38, No. 3, 8053, 2003.
12. Zhao, X.-F. and S.-X. Huang, "Refractivity from clutter by variational adjoint approach," *Progress In Electromagnetics Research B*, Vol. 33, 153–174, 2011.
13. Douvenot, R., V. Fabbro, P. Gerstoft, et al., "Real time refractivity from clutter using a best fit approach improved with

- physical information,” *Radio Sci.*, Vol. 45, RS1007, 2010.
14. Zhang, J.-P., Z.-S. Wu, and R.-X. Hu, “Combined estimation of low-altitude radio refractivity based on sea clutters from multiple shipboard radars,” *Journal of Electromagnetic Waves and Applications*, Vol. 25, Nos. 8–9, 1201–1212, 2011.
  15. Yardim, C., P. Gerstoft, and W. S. Hodgkiss, “Tracking atmospheric ducts using radar clutter: evaporation duct tracking using Kalman filters,” *International Symposium on Antennas and Propagation Society*, 4609–4612, Honolulu, HI, Jun. 9–15, 2007.
  16. Yardim, C., P. Gerstoft, and W. S. Hodgkiss, “Evaporation duct estimation from clutter using meteorological statistics,” *International Symposium on Antennas and Propagation Society*, 1–4, San Diego, CA, Jul. 5–11, 2008.
  17. Yardim, C., P. Gerstoft, and W. S. Hodgkiss, “Sensitivity analysis and performance estimation of refractivity from clutter techniques,” *Radio Sci.*, Vol. 44, RS1008, 2009.
  18. Karimian, A., C. Yardim, P. Gerstoft, et al., “Refractivity estimation from sea clutter: An invited review,” *Radio Sci.*, Vol. 46, RS6013, 2011.
  19. Wang, B., Z.-S. Wu, Z.-W. Zhao, et al., “Retrieving evaporation duct heights from radar sea clutter using particle swarm optimization (PSO) algorithm,” *Progress In Electromagnetics Research M*, Vol. 9, 79–91, 2009.
  20. Hall, M. P. M., *Effects of the Troposphere on Radio Communication*, Peter Peregrinus Ltd., Stevenage, 1979.
  21. Sirkova, I., “Brief review on PE method application to propagation channel modeling in sea environment,” *Central European Journal of Engineering*, 1–20, 2011.
  22. Zhao, X.-L., J.-Y. Huang, and S.-H. Gong, “Modeling on multi-eigenpath channel in marine atmospheric duct,” *Radio Sci.*, Vol. 44, RS1009, 2009.
  23. Zhang, J.-P., Z.-S. Wu, Q.-L. Zhu, et al., “A four-parameter M-profile model for the evaporation duct estimation from radar clutter,” *Progress In Electromagnetics Research*, Vol. 114, 353–368, 2011.
  24. Wang, A.-Q., L.-X. Guo, and C. Chai, “Numerical simulations of electromagnetic scattering from 2D rough surface: Geometric modeling by nurbs surface,” *Journal of Electromagnetic Waves and Applications*, Vol. 24, No. 10, 1315–1328, 2010.
  25. Qi, C., Z. Zhao, W. Yang, et al., “Electromagnetic scattering and doppler analysis of three-dimensional breaking wave crests at low-

- grazing angles,” *Progress In Electromagnetics Research*, Vol. 119, 239–252, 2011.
26. Chen, Z., C. Zhao, Y. Jiang, et al., “Wave measurements with multi-frequency HF radar in the east china sea,” *Journal of Electromagnetic Waves and Applications*, Vol. 25, No. 7, 1031–1043, 2011.
  27. Li, J., L.-X. Guo, and H. Zeng, “FDTD method investigation on the polarimetric scattering from 2-D rough surface,” *Progress In Electromagnetics Research*, Vol. 101, 173–188, 2010.
  28. Luo, W., M. Zhang, C. Wang, and H.-C. Yin, “Investigation of low-grazing-angle microwave backscattering from three-dimensional breaking sea waves,” *Progress In Electromagnetics Research*, Vol. 119, 279–298, 2011.
  29. Guo, L.-X., Y. Liang, et al., “A high order integral SPM for the conducting rough surface scattering with the tapered wave incidence-TE case,” *Progress In Electromagnetics Research*, Vol. 114, 333–352, 2011.
  30. Sirkova, I., “Propagation factor and path loss simulation results for two rough surface reflection coefficients applied to the microwave ducting propagation over the sea,” *Progress In Electromagnetics Research M*, Vol. 17, 151–166, 2011.
  31. Kuttler, J. R. and G. D. Dockery, “Theoretical description of the parabolic approximation/fourier split-step method of representing electromagnetic propagation in the troposphere,” *Radio Sci.*, Vol. 26, No. 2, 381–393, 1991.
  32. Levy, M. F., *Parabolic Equation Methods for Electromagnetic Wave Propagation*, The Institution of Electrical Engineers, London, 2000.
  33. Dockery, G. D. and J. R. Kuttler, “An improved impedance-boundary algorithm for fourier split-step solutions of the parabolic wave equation,” *IEEE Trans. Antennas Propag.*, Vol. 44, No. 12, 1592–1599, 1996.
  34. Clerc, M., *Particle Swarm Optimization*, ISTE Publishing Company, London, 2006.
  35. Wang, J., B. Yang, S. H. Wu, and J. S. Chen, “A novel binary particle swarm optimization with feedback for synthesizing thinned planar arrays,” *Journal of Electromagnetic Waves and Applications*, Vol. 25, Nos. 14–15, 1985–1998, 2011.